SYNTHESIS OF PLATINUM NANOPARTICLES ON GRAPHENE VIA ELECTROPHORETIC DEPOSITION AS CATALYST FOR PEMFC

by

MUHAMMAD FAISAL JAMIL

Submitted to the Graduate School of Engineering and Natural Sciences

in partial fulfillment of the requirements for the degree of

Master of Science

Sabancı University

July 2017

SYNTHESIS OF PLATINUM NANOPARTICLES ON GRAPHENE VIA ELECTROPHORETIC DEPOSITION AS CATALYST FOR PEMFC

APPROVED BY:

Assoc. Prof. Dr. Selmiye Alkan Gürsel .....

(Thesis supervisor)

Assist. Prof. Dr. Alp Yürüm .....

Assoc. Prof. Dr. Önder Metin .....

DATE OF APPROVAL: 31-07-2017 .....

ABSTRACT

SYNTHESIS OF PLATINUM NANOPARTICLES ON GRAPHENE VIA ELECTROPHORETIC DEPOSITION AS CATALYST FOR PEMFC

MUHAMMAD FAISAL JAMIL

Materials Science and Engineering M.Sc. Thesis, July 2017

Supervisor: Assoc. Prof. Dr. Selmiye Alkan Gürsel

Keywords: Electrophoretic deposition, graphene, platinum, PEMFC, graphene oxide

High Pt loadings have better tradeoff in PEMFC in terms of improved performance and operational longevity, but to employ low amounts of Pt electrocatalysts and augment its utilization is vital. This study presents the use of a novel technique, an anodic electrophoretic deposition (EPD) method, through which Pt/GO nanocomposites have been successfully fabricated onto oxygen plasma pretreated carbon paper in an organo-aqueous media. Characterization of the prepared Pt/GO samples is done via Raman spectroscopy, field emission scanning electron microscopy, x-ray photoelectron spectroscopy, inductively coupled plasma, focused ion beam, transmission electron microscopy, and cyclic voltammetry. Electrochemically active surface area results (optimal ECSA value, 27 m^2/g of Pt) calculated from the prepared samples reveal high performance of Pt nanoparticles

dispersed well on GO at lower loadings (0.129 mg/cm^2), displaying their synergistic performance making them potential catalyst candidate for PEMFC.

ÖZET

PEMFC KATALİZÖRÜ OLARAK PLATİN NANOPARÇACIKLARININ GRAFEN ÜZERİNDE ELEKTROFORETİK KAPLAMA YÖNTEMI İLE SENTEZİ

MUHAMMAD FAISAL JAMIL

Malzeme Bilimi ve Mühendisliği Yüksek Lisans Tezi, Temmuz 2017

Tez Danışmanı: Doç. Dr. Selmiye Alkan Gürsel

Anahtar Kelimeler: Elektroforetik kaplama, grafen, platin, PEMFC, grafen oksit

Yüksek Pt yüklemeleri PEMFC için performansının iyileştirilmesi ve uzun ömürlü olması açısından gereklidir. Ancak düşük Pt elektrokatalizör yüklemeleri ve etkin kullanımı gerekmektedir. Bu çalışmada özgün bir teknik olan anodik elektroforetik kaplama (EPD) metodu kullanılarak Pt/GO nanokompozitleri; önceden oksijen plazma uygulanmış karbon kağıt üzerine organik-sulu ortamda başarılı bir şekilde kaplanmıştır. Hazırlanan Pt/GO örnekleri fiziksel teknikler olan; Raman spektroskopi, taramalı elektron mikroskopisi, X-ışını fotoelektron spektroskopisi, endüktif eşleşmiş plazma, odaklanmış iyon demeti, geçirimli elektron mikroskopisi ve dönüşümlü voltametre ile karakterize edilmiştir. Hazırlanan örnekler için hesaplanan elektrokimyasal aktif yüzey alanı sonuçları (optimum ECSA değeri 27 m^2/g Pt), GO yüzeyinde dağılmış olan düşük miktarda yüklenmiş Pt nanoparçacıklarının (0.129 mg/cm^2) yüksek performans gösterdiği ve burada sunulan sentez yöntemi ile üretilen örneklerin PEMFC için potansiyel katalizör olacağını ortaya çıkarmıştır.

Dedicated to my beloved parents and siblings.

ACKNOWLEDGEMENTS

I am honored and obliged to be the student of Assoc. Prof. Dr. Selmiye Alkan Gürsel, my supervisor. I am grateful to her for her technical, scientific and moral support which intrinsically motivated me to work diligently for this master's thesis. I am also indebted to my co-supervisor, Dr. Emre Biçer, for his professional support and encouragement. I would like to extend my gratitude to the jury, Assist. Prof. Dr. Alp Yürüm and Assoc. Prof. Dr. Önder Metin, for their time in reviewing and commenting on my thesis.

I am thankful to the faculty of Materials Science and Engineering who taught me the knowledge essential to understand the basic concepts and excel in adjunct sciences, especially, Prof. Dr. Mehmet Ali Gülgün, Assoc. Prof. Dr. İ. Burç Mısırlıoğlu, Prof. Dr. Yuda Yürüm, Prof. Dr. Melih Papila, and Assoc. Prof. Dr. Selmiye Alkan Gürsel.

I am grateful to the EU's 7^{th} Framework Programme under grant agreement N° 604391 Graphene Flagship for their funding. Also, I would like to thank East Anatolia High Technology Application and Research Center (DAYTAM) for their help in TEM and XPS characterizations.

I would like to thank my younger brother, Esaam Jamil, for his persuasive encouragement and feedback. Also, I am thankful to my colleagues and FENS staff members: Adnan Taşdemir, Ali Tufani, Ali Ansari, Sirous Khabbazabkenar, Ashish Pandey, Parveen Qureshi, Mahdieh Shakoorioskooie, Navid Haghmoradi, Emre Burak Boz, Zeki Semih Pehlivan, Begüm Yarar, Yonca Belce, Dr. Özlem Karahan, Dr. Meltem Sezen, Dr. Feray Bakan, Mr. Turgay Gönül, and Ms. Sibel Pürçüklü.

TABLE OF CONTENTS

LIST OF FIGURES

LIST OF TABLES

ABBREVIATIONS AND SYMBOLS

AFC:	Alkaline fuel cells
CE:	Counter electrode
CH_3OH:	Methanol
CO:	Carbon monoxide
CO_2:	Carbon dioxide
CV:	Cyclic voltammetry
CVD:	Chemical vapor deposition
DMFC:	Direct methanol fuel cells
DSSC:	Dye-sensitized solar cells
E:	Young's Modulus
ECSA:	Electrochemically active surface area
EDS:	Energy dispersive spectroscopy
EPD:	Electrophoretic deposition
FE-SEM:	Field emission scanning electron microscopy
FIB:	Focused ion beam
GO:	Graphene oxide
H_2:	Hydrogen
H^+:	Proton
HCPA:	Hexachloroplatinic acid
HOR:	Hydrogen oxidation reaction
ICP:	Inductively coupled plasma
IPA:	Isopropyl alcohol

ITO:	Indium tin oxide
IUPAC:	International Union of Pure and Applied Chemistry
MCFC:	Molten carbonate fuel cells
MEA:	Membrane electrode assembly
O_2:	Oxygen
OH^-:	Hydroxyl group
ORR:	Oxidation reduction reaction
PAFC:	Phosphoric acid fuel cell/s
PEFC:	Polymer electrolyte fuel cell
PEMFC:	Proton exchange membrane fuel cell/s
PGM:	Pt-group metals
Pt:	Platinum
Pt/GO/CP:	Pt-graphene oxide nanocomposites on carbon paper
RE:	Reference electrode
RFC:	Reversible fuel cells
rGO:	Reduced graphene oxide
SCE:	Saturated calomel electrode
SOFC:	Solid oxide fuel cells
SPFC:	Solid polymer fuel cell
TEM:	Transmission electron microscopy
TPB:	Triple phase boundary
WE:	Working electrode
XPS:	X-ray photoelectron spectroscopy

1. Introduction

Since the dawn of modern civilization, mankind's energy needs have been catered by the consumption of fossil fuels, petroleum, and natural gas, causing these natural energy reservoirs to dwindle at an alarming rate. In addition, the aftermath of burning these fossils have resulted in an increased level of greenhouse gases and global warming. Globally, there is a dire need to generate an alternative renewable energy source which is environmentally friendly and has zero to low carbon footprint so that adverse effects on the health, climate, and economy can be avoided [1].

1.1. Fuel Cells

Keeping in view the aforementioned requirements for an alternative energy source, fuel cells have been exploited extensively because of their capability to produce power in a clean manner with no emissions of greenhouse gases or consumption of fossils [1, 2], and generating only electricity with water, heat [1], and negligible amounts of CO_2 [3] as by-products. Historically, Sir Humphrey Davy in 1802 created a simple fuel cell, followed by the revolutionary work of the scientist Christian Friedrich Schönbein in 1838. In general, Sir William Grove is accredited for pioneering first fuel cell in 1839 which he called the "gas battery". With the passage of time, this technology progressed but it wasn't on a par with the internal combustion engines which dominated the industrial era. In 1889, the terminology "fuel cell" was first used by Charles Langer and Ludwig Mond whose research was based on using coal gas as a fuel [4, 5]. The fuel cell industry is still evolving, despite years of research and development [6].

A fuel cell is an electrochemical device that operates at various temperature ranges and continuously converts chemical energy into an electrical energy [1]. Basic mechanism in a fuel cell involves electrolysis reaction. H_2 is injected into the "fuel electrode" and O_2 is injected into the "air electrode". H_2 is oxidized to protons (H^+), while O_2 is reduced to hydroxyl ions (OH^-). Both chemical species react with each in the electrolyte to form water. The electrons generated from the oxidation of H_2 gas at the anode are taken to the external circuit before returning to the cathode for further generation of OH^- (Figure 1) [4].

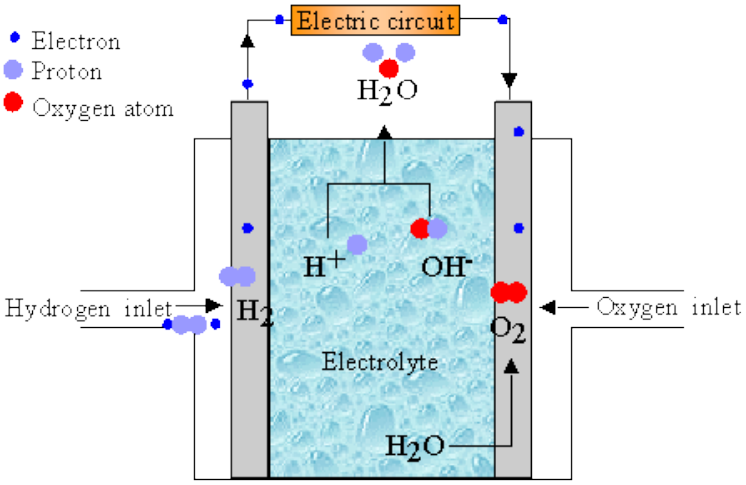

Figure 1. Representation of a basic fuel cell [4].

Fuel cells are classified mainly by the type of electrolyte they utilize [7]. These power generation devices have found uses in stationary applications, as portable power sources [8, 9], in electric vehicles, and portable electronic devices [10]. Different kinds of fuel cells are: direct methanol fuel cells (DMFC), proton exchange membrane fuel cells (PEMFC), alkaline fuel cells (AFC), phosphoric acid fuel cells (PAFC), molten carbonate fuel cells (MCFC), solid oxide fuel cells (SOFC), and reversible fuel cells (RFC) [7] (Figure 2) [11].

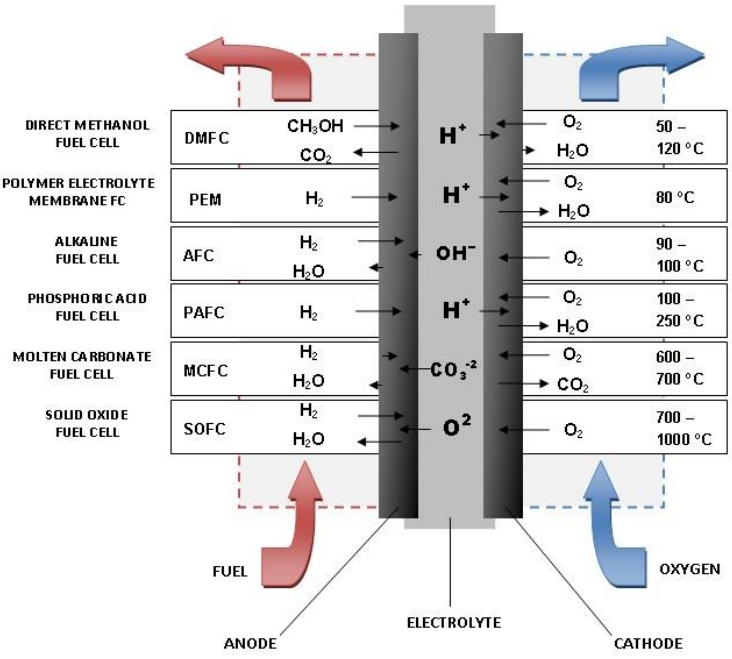

Figure 2. Different kinds of fuel cells have unique fuel intakes and electrochemical reactions [11].

1.2. PEMFC

The concept of fuel cell was not completely developed till the 1950s when a "high energy/density" system was required for the space programme [12]. In 1960s, General Electric (U. S. A.) first developed the PEMFC, also called as solid polymer fuel cell (SPFC) [13] and polymer electrolyte fuel cell (PEFC) [10, 14, 15], for NASA's first manned space vehicles [13]. Based on the fuel, PEMFC can be categorized into two types: one that runs on H_2; and the other runs on CH_3OH, called as DMFC [1]. Both these types of fuel cells have similar MEA, but demonstrate a diverse degree of performance [12]. An MEA is the heart of PEMFC, it consists of an electrolyte membrane and two catalyst layers [14]. The chemical reactions that take place on the catalyst layer in a PEMFC are as follows [12] and are diagrammatically represented in (Figure 3) [7], equations (i, ii, iii):

At anode:	$2H_2 \rightarrow 4H^+ + 4e^-$	$(E^0_a = 0.00\ V)$	(i)
At cathode:	$O_2 + 4H^+ + 4e^- \rightarrow 2H_2O$	$(E^0_c = 1.230\ V)$	(ii)
Overall:	$2H_2 + O_2 \rightarrow 2H_2O$	$(E^0_{cell} = 1.230\ V)$	(iii)

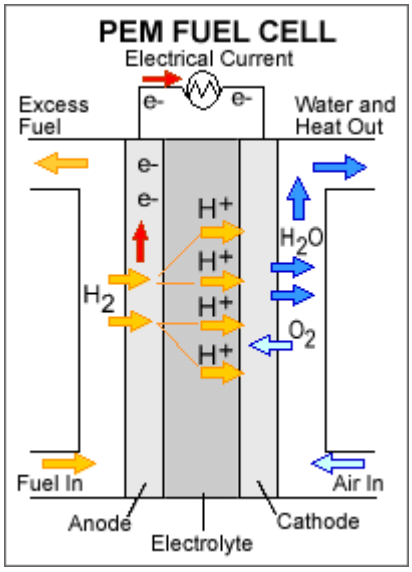

Figure 3. Diagrammatical representation of PEMFC reactions [7].

PEMFC are quite promising as they offer several advantages: low noise [3]; high energy conversion efficiency [3, 14]; high power density [14, 16-18]; low operating temperature [10, 11, 13, 16-20]; low weight, compactness, and long stack life [17]; quick start-ups [13, 19] and aptness for

intermittent operation [17]. Further advantages of PEMFC include no corrosive fluid hazards and working in any orientation [13]. This makes PEMFC extremely suitable for use in vehicles [11, 13, 21], transportation [3], portable power generation [3, 13], and backup power units [1]. Commercialization of PEMFC as opposed to conventional energy sources is still a challenge. Thanks to the research in past few years, PEMFC have transitioned from prototype to commercial products, but still cost reduction and technological challenges persist [17, 22]. This impediment to the commercialization is mainly due to inclusive fuel cell stack cost [16] which is attributed to high cost of noble metal catalyst, usually Pt [3, 8, 14, 16, 17, 23-27] and Pt-group metals (PGM) [23], low Pt utilization in the catalyst layer [23, 28], and long term fuel cell stability [3] and durability [8].

1.3. Catalyst Support

The aim of employing carbon-based nanomaterials as catalyst support in PEMFC is to reduce the amount of noble metal usage and to enhance its utilization [29] and electrochemical activity [3]. In addition, catalyst supports assist in effective collection and transfer of electrons [3, 29-31] to the collecting electrode surface [17, 31]. To attain high dispersion and maximum utilization of Pt-electrocatalysts for PEMFC, an appropriate catalyst support is needed [32]. In general, there are four requirements for such a suitable catalyst support, namely, high surface area, suitable porosity, high stability, and high electrical conductivity [32].

1.4. Graphene

From the pool of catalyst supports, carbon-based materials have been potential catalyst support candidates for PEMFC. And among different carbon-based catalyst support materials, graphene is an excellent choice material. It has recently attracted the attention in scientific community due to its fascinating properties [31-36] which justifies its nickname of "miracle material" [37]. IUPAC commission recommended the name "graphene" for single carbon layer structure. Previously used terminology "graphite layers" was discontinued as they stood for three-dimensional stacking structure known as "graphite" [8]. Graphene, known as graphene oxide (GO) [38], is a two-dimensional nanomaterial [27, 32, 33, 35, 39-47] comprised of monolayer [48] of covalently bonded [41, 48] carbon atoms [32, 35], sp^2 hybridized [27, 31, 39, 40, 44] and packed in a hexagonal lattice [33, 35, 39, 40, 43, 47]. GO has several oxygen containing functional

groups, for instance, hydroxy and epoxy groups positioned on its basal plane, along with carboxyl, phenol and ketone groups located at the edges [40, 49-52] (Figure 4) [40].

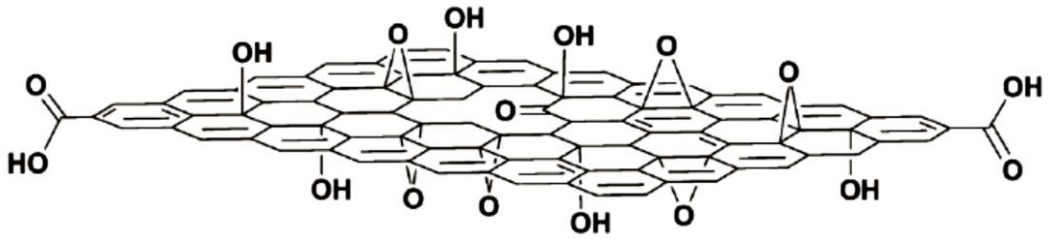

Figure 4. Chemical structure of a monolayer GO [40].

Graphene fulfills the four general requirements necessary for a catalyst support in a PEMFC. It has high planar surface area (calculated values, 2600 - 2630 m^2/g) [27, 40, 46, 48, 53, 54], superior mechanical strength (Young's Modulus, E = 1.0 - 1.02 TPa) [40, 41, 48], high carrier mobility (10000 cm^2/Vs [40] to 15000 cm^2/Vs [48]), high thermal conductivity (5000 W/mK) [40, 48], unique graphitized basal plane structure [46, 55], excellent chemical stability [34, 44, 48, 55, 56], and outstanding electrical conductivity (64 mS/cm) [27]. Due to the aforementioned robust mechanical and physical properties of graphene, noble metal nanoparticles, especially Pt had been deposited on graphene and employed as an electrode material in fuel cells [32]. The rationale for the incorporation of graphene as a support material for Pt nanoparticles is justified as following: graphene strongly interacts with Pt on nanometer scale leading to the decrement in platinum's size and increases platinum's catalytic activity [37]; to employ graphene's high electronic mobility and in anchoring Pt nanoparticles for enhanced electrochemical reactions in a synergistical manner [6, 31, 32]; and graphene when used as a conductive support, increases Pt catalyst's utilization coefficient by improving the interfacial properties between the electrolyte and the catalyst [32, 46].

1.5. Platinum as Electrocatalyst

Most frequently used catalysts for PEMFC are Pt and Pt-alloy nanoparticles supported on activated carbon with high specific surface [3, 19, 57]. Because of low availability [17, 26] and high cost of Pt metal as catalyst in PEMFC, as mentioned earlier, it is imperative to reduce Pt loading [17]. In the initial days of PEMFC development, Pt loading was 28 mg/cm^2 [13]. The target set by the U.S. Department of Energy for the year 2017 for Pt loading as fuel cell catalyst is ≤ 0.125 mg/cm^2 of electrode area [58]. Pt's catalytic activity depends on few factors,

namely, its particle size, supporting materials, and preparation method [57]. Theoretically, to improve Pt utilization, reduction in its size is necessary which in the literature has been reported between 2 and 6 nm [3]. The electrochemical reactions occurring in the PEMFC can only take place at the spatially limited sites where catalyst, electrolyte, and fuel gas contact each other. These specific sites are known as "triple-phase boundaries" (TPB) [13, 14, 59] (Figure 5) [14].

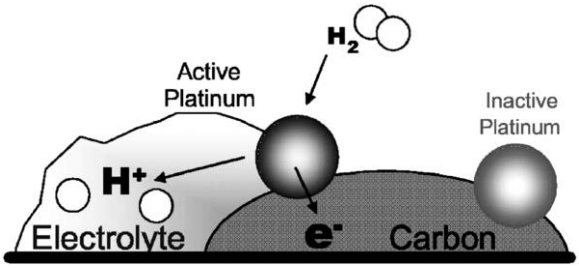

Figure 5. Graphic illustration of a triple-phase boundary [14].

Further reduction in Pt catalyst nanoparticle size i.e. smaller than 2 nm, is not feasible because the nanoparticles would merge into the micro pores of the supporting material and eventually leading to inaccessibility of the reactants to the Pt [28] due to lack of TPB [3]. In a PEMFC, Pt is used as a catalyst for anode and cathode [13]. At the anode, it works as a catalyst for hydrogen oxidation reaction (HOR), and at the cathode it works as a catalyst for oxidation reduction reaction (ORR) [22, 60]. During the anode processes, the incoming H_2 gas is adsorbed onto the surface of Pt which results in cleavage of H-H bond producing adsorbed hydrogen [19], equation (iv):

$$\tfrac{1}{2}\, H_2 + * \rightarrow H^* \qquad \text{(iv)}$$

(where * denotes surface site)

Due to this oxidation step, each adsorbed hydrogen loses an electron resulting in hydrogen leaving the surface as protons (H^+) [19] , equation (v):

$$H^* \rightarrow H^+ + * + e^- \qquad \text{(v)}$$

The reaction kinetics of HOR are very fast even at low Pt loadings as compared to that of ORR, which are quite slow and require higher Pt loadings [9]. The ORR occurring at the cathode is responsible for more than half of PEMFC's voltage loss and is a major

challenge because the catalyst is susceptible to extremely harsh chemical environment in the fuel cell [9] and yet should be chemically active to activate O_2. The ORR can occur via two mechanisms in PEMFC's acidic media, namely, dissociative and associative pathways, respectively. They are explained as follows [19]:

I. In a dissociative pathway, the incoming oxygen from the cathode is adsorbed onto the Pt surface which results in cleavage of O-O bond leading to the formation of adsorbed oxygen atoms, equation (vi):

$$\frac{1}{2} O_2 + * \rightarrow O* \quad \text{(vi)}$$

These adsorbed oxygen atoms are then protonated by the inbound H^+ from the HOR, and are reduced by the incoming flow of electrons to form surface bound hydroxy groups (OH*), equation (vii):

$$O* + H^+ + e^- \rightarrow OH* \quad \text{(vii)}$$

This surface bound hydroxy group is further reduced and protonated, resulting in the generation of water which leaves the Pt surface (see Figure 3), equation (viii):

$$OH* + H^+ + e^- \rightarrow H_2O + * \quad \text{(viii)}$$

II. In an associative mechanism, oxygen molecule double bonds do not cleave, instead O_2 is adsorbed onto the Pt surface, equations (ix, x):

$$O_2 + * \rightarrow O_2* \quad \text{(ix)}$$

$$O_2* + H^+ + e^- \rightarrow HO_2* \quad \text{(x)}$$

The reaction proceeds further via "two electrons" route forming hydrogen peroxide as follows, equation (xi):

$$HO_2* + H^+ + e^- \rightarrow H_2O_2* \quad \text{(xi)}$$

The surface bound H_2O_2 additionally might react or desorb, equation (xii):

$$H_2O_2* \rightarrow H_2O_2 + * \quad \text{(xii)}$$

The formation of H_2O_2 in a PEMFC is quite unfavorable as it permeates the proton exchange membrane and causes "radical oxidative" degradation of the membrane [19].

On the contrary, Pt electrocatalysts are also vulnerable to poisoning in the PEMFC, especially due to sulfur species and CO. Among the Pt-group metals (PGM), Pt is one of the best noble metal capable of being stable and poisoning resistant in PEMFC's harsh chemical environment [3, 19] and capable of being selective in following the dissociative pathway for ORR at the cathode [19].

1.6. Electrophoretic Deposition

In the literature, different approaches have been employed for the preparation of graphene-nanoparticle composites. These include reduction method [61], hydrothermal method [62], ex-situ method [63], and electrochemical method [64]. Electrochemical method has several advantages over other methods. To name a few, low cost [40, 65], highly reproducible, simple, fast [49], green technique [40, 49], and ease-of-operation [65]. One of the most efficient electrochemical deposition method for the preparation of graphene and graphene based films and electrodes is electrophoretic deposition (EPD) [43, 52, 56, 66-68]. In addition, this technique has also been extensively used for the electrodeposition of Pt nanoparticles as well [69]. Historically, the first known EPD process was discovered in 1808 by a scientist, Ruess, who observed that the clay particles in aqueous media moved when an electric field was applied. But the first real application of an EPD technique was seen in 1933 when a patent for the "deposition of thoria particles on a Pt cathode as an emitter for electron tube application" was filed in the U.S. [70].

EPD is a solution based technique that is based on electrophoresis of charged particles under the influence of an electric field [35, 42]. EPD has two-step mechanism processes which

involves the movement of charged particles towards the oppositely charged electrodes per potential gradient generated in the solution by using two electrodes, followed by assemblage of the particles at the electrode surface and forming a deposit [10, 14, 45, 52, 71]. EPD can be categorized in two kinds, namely, anodic and cathodic EPD. When negatively charged colloidal particles in the solution deposit on the anode, it is termed as an anodic EPD. On the other hand, in cathodic EPD, positively charged colloidal particles in the solution are deposited on the cathode [42, 52] (Figure 6) [70].

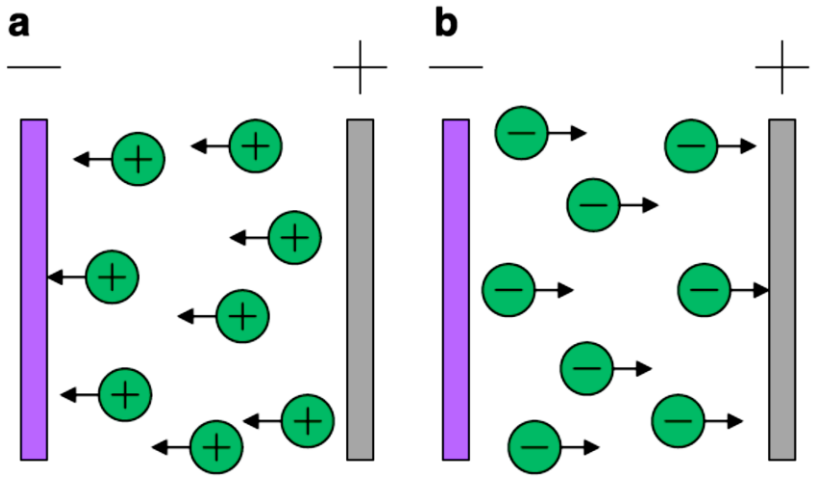

Figure 6. Graphic representation of (a) cathodic EPD and (b) anodic EPD [70].

An appropriate medium is required for the steady dispersion of particles in an EPD bath. Either organic solvents, for instance, ketones, alcohols, and amides are utilized or an aqueous media is employed. Both these mediums can be used based on preferences and limitations. For example, organic solvents are preferred because of their high density, better chemical stability and low conductivity [43, 52], but their use is often times limited due to cost, toxicity, and flammability [43]. Conversely, aqueous suspensions in EPD are employed because they are environment friendly and very economical [43, 52]. Nevertheless, at higher voltage ranges the aqueous media is prone to electrolysis and evolution of gases at the electrodes occurs, thereby damaging the deposits [35]. The benefits of EPD are uniform deposition of charged particles [14, 34, 35, 43, 55, 68, 72], control of film morphology [52, 72], good thickness controllability [14, 34, 35, 43, 52, 55, 66, 68, 71], size scalability [35, 52], high dense packing of deposit [35, 52, 55], deposition at room temperature [35, 52], and simplicity and cost-effectiveness [35, 42, 43, 52, 55, 71]. The ability of EPD to control morphology and nucleation density demonstrates its superior

capability for the preparation of nano-sized electrocatalysts with even distribution [73] on the support material necessary for efficient and long-lasting performance of PEMFC.

The EPD of graphene predates the isolation of mono layers of graphene in 2004 by Novoselov *et al.* [74]. In 2001, the first know synthesis of single graphene sheets via EPD was reported by Affoune *et al.* [75]. Their process involved electrophoretic deposition of diamond nanoparticles, suspended in an isopropyl alcohol media with additives, on highly oriented pyrolytic graphite (HOPG) followed by annealing at 1600°C in an Ar environment for 30 minutes. Because of this EPD method, "nano-sized" graphene with an inter-layer distance of 0.35 - 0.37 nm were formed.

Ishikawa *et al.* [76] described the electrophoretic deposition of highly stacked graphene films onto an insulating glass substrate. They demonstrated successful deposition of GO flakes at 10 V/5 minutes onto an oxygen plasma pretreated insulating glass substrate (working electrode, whose surface was attached to a Cu-tape) placed 5 mm apart from the Pt plate (counter electrode). Without further post treatment reduction process and complicated transfer processes, they claimed that GO was in-situ reduced during EPD, which is ideal for usage in graphene based transparent conductive films.

Hasan *et al.* [77] reported an EPD scheme using an aqueous media to synthesize large-area films of GO. Fine tuning of the EPD parameters resulted in the formation of different morphological GO structures. For instance, it was observed that at higher voltage range and low pH, cathodic deposition was more dominant which was also observed by Ordikhani *et al.* [78]. The cathodic EPD of GO had "brick" like microstructure, while anodically deposited GO had "rug" morphology. The use of sacrificial layer procedure for the formation of "free-standing" GO films was advantageous as the obtained GO films could be deposited on various substrates.

Choi *et al.* [79] reported a fabrication process that involved EPD of graphene on fluorine-doped tin oxide glass using an aqueous media. It was found that film thickness was a direct function of deposition time. The fabricated graphene based electrodes tested in dye-sensitized solar cells (DSSCs) showed optical transmittance values of up to 80% with an energy conversion of 2.3%. It was found out that at higher deposition time, more graphene

layers were deposited resulting in sharp decrease in transmittance values. Hence, tunability is the key to produce optimized electrodes.

The work of Liu *et al.* [49] is quite interesting because of its relevance to fuel cell catalysts. They reported a simple two step cathodic EPD process for the deposition of GO onto indium tin oxide (ITO) glass electrodes in which GO was reduced, followed by a second step involving EPD of Pt nanoparticles onto the reduced GO (rGO) films. Electrochemical testing revealed that Pt/rGO films outperformed Pt/GO in terms of electrocatalytic activity and stability for CH_3OH oxidation. This increase in performance is due to rGO's large surface area and better electrical conductivity alongside Pt nanoparticles' exceptional catalytic activity.

Another example involving the development of PEMFC catalyst is by Seger *et al.* [31]. They electrophoretically deposited partially reduced GO-Pt films onto glassy carbon and carbon Toray paper. The deposited films were subjected to chemical reduction (using hydrazine) and then annealed at 300°C/8 hours to eliminate hydrazine. As a result, reduced GO-Pt nanocomposites were formed. These developed films showed an astounding 77% increment in ECSA values. Nevertheless, evaluation of the films when employed in a fuel cell showed massive declination in power output. This poor performance is possibly ascribed to the loss of H^+ conductivity property of Nafion ionomers.

Fabrication and end use of nanocomposites dictate which type of EPD is pertinent. For instance, Liu *et al.* [54] used an anodic EPD technique to deposit GO from an aqueous suspension onto ITO glass sheets followed by a supplementary step i.e. in-situ reduction of deposited GO sheets via constant potential reduction method. Characterization results revealed that this additional in-situ reduction process did not distort the morphology of rGO. Furthermore, the obtained films exhibited excellent performance (calculated specific capacitance was 156 F/g at 150 mA/g) and stability making them viable candidates for supercapacitors.

Xia *et al.* [80] deposited graphene electrophoretically onto porous 3D NiO for the fabrication of supercapacitors, and found an increased capacity retention (up to 94%) and improved specific capacitance. The addition of magnesium nitrate hexahydrate in the stable GO solution shifted suspension charge neutrality to positive followed by instant deposition

of GO onto the Ni-foam substrate. The EPD GO/NiO films showed exceptional pseudocapacitance values of 400 and 324 F/g at 2 and 40 A/g, respectively, and kept 94% of capacitance retention over 2000 cycles.

In another work on fabrication of supercapacitors, Wu *et al.* [56] employed single step EPD in which GO nanosheets were dispersed in IPA with the addition of $Ni(NO_3)_2$ and were deposited on stainless steel substrate and subsequently annealed at 300°C/1 hour. EPD resulted in an in-situ reduction of Ni ions and the subsequent heat treatment oxidized these Ni ions to nickel oxide. The incorporation of NiO on GO resulted in higher specific capacitance of up to 569 F/g, which is 40 times higher than that of the bare GO electrode (13 F/g) at a discharge current density of 5 A/g.

Saminathan *et al.* [16] have reported an EPD process in which Pt nanoparticles were deposited over multi walled carbon nano tubes which were in-situ grown via chemical vapor deposition (CVD). The EPD setup consisted of Pt mesh as counter electrode and an SCE as reference electrode. Uniform deposition and optimized Pt loading of 0.13 mg/cm^2 was achieved at -0.6 V vs. SCE. Fuel cell test results revealed a peak power density of 640 mW/cm^2 at 80°C and 101 kPa. Thus, achieving high power density at lower Pt loading makes these electrodes suitable candidates for PEMFC.

1.7. Objectives of Present Work

Over the past decades, research has been intensely focused on cutting down PEMFC manufacturing costs which involved numerous factors, such as decreasing Pt loading, improving Pt catalyst utilization, developing stable proton exchange membranes, and employing chemically stable catalyst supports, etc. Several methods have been proposed for the manufacturing of Pt and Pt-co particulate as catalysts on carbon based support for use in PEMFC, and have demonstrated better performance as well. But the complexities involved in the manufacturing process, loss in power output and degradation in longer run have raised red flags. More knowledge is crucial to understand the basics of ongoing changes within the matrix of developed protocols. No doubt traditionally available carbon based materials have been widely employed in PEMFC, especially carbon black, making it commercially viable, but the search for better substitute materials demanded a breakthrough. Until the discovery of graphene back in 2004 by Novoselov *et al.* [74], the introduction of 2D materials opened a whole new chapter with endless application possibilities. Graphene because of its high planar surface area, superior mechanical strength, high carrier mobility, excellent chemical stability, and electrical conductivity make it an ideal candidate as catalyst support for fuel cells. In the literature, different synthesis methods exist, to name a few, chemical reduction, CVD, hydrothermal, ex-situ methods, etc. These methods have been employed to develop nanocomposites, but they too have demerits, for instance, complex procedures involved, toxicity of the chemicals used, and are responsible for environmental hazards, etc. Thus, it is imperative to come up with an alternative and green solution. Hence, EPD method, which have been employed as a plating technique in the industry, can be tested as potential synthesis tool. The rationale for choosing this method lies in its ease of operation, simplicity, controlled film morphology, and cost effectiveness. Just like other deposition or synthesis processes, the optimization of parameters is necessary to achieve desired nanocomposites. The ability of EPD to control morphology and nucleation density demonstrates its superior capability for the preparation of nano-sized electrocatalysts with even distribution [73] on the support material necessary for efficient and long-lasting performance of PEMFC.

Initially, in this work several optimization steps were involved:

I. Cathodic EPD of Pt (chloroplatinic acid hexahydrate) on AvCarb® MGL190 carbon paper in N,N-Dimethylformamide and tetrabutylammonium tetrafluoroborate media.
II. Switching to anodic EPD, and depositing Pt nanocomposites on AvCarb® MGL190 carbon paper over whole voltage range i.e. 1 to 32 V/5 minutes in above mentioned organic media.
III. Optimizing the deposition voltages based of cyclic voltammograms.
IV. Anodic EPD of Pt on indium tin oxide in the organic media at various voltages i.e. 2, 3, 4, and 5 V/10 minutes, respectively, followed by CV.
V. Anodic EPD of Pt (chloroplatinic acid hexahydrate and tetrabutylammonium tetrafluoroborate) on oxygen plasma pre-treated AvCarb® MGL190 carbon paper at different voltages i.e. 3 to 8 V/10 minutes.
VI. Anodic EPD of GO (concentration, 0.6 mg/mL of organo-aqueous solvent of 1:1 w/w ethanol:water) on ITO at 4 to 10 V/10 minutes.
VII. Anodic EPD of GO (concentration, 1.5 mg/mL of organo-aqueous solvent of 1:1 w/w ethanol:water) and Pt (from chloroplatinic acid hexahydrate) on ITO at 10 V/40 minutes.
VIII. Anodic EPD of GO/Pt (GO concentration, 0.6 and 1.5 mg/mL) on oxygen plasma pre-treated AvCarb® MGL190 carbon paper at 10 V/40 minutes.
IX. Finally, anodic EPD of GO/Pt (GO concentration, 1.5 mg/mL) on oxygen plasma pre-treated AvCarb® MGL190 carbon paper at 10 V/80, 120, 240, and 300 minutes (details are available in the experimental part).

In this work, we report the fabrication of a catalyst layer based on Pt-GO nanocomposites on carbon paper (Pt/GO/CP). These nanocomposites were prepared using one-step anodic EPD technique, involving simultaneous deposition of Pt nanoparticles and GO onto oxygen plasma pre-treated carbon paper in an organo-aqueous media at various deposition time. A graphic representation of the EPD process is presented in Figure 7. The prepared Pt/GO/CP were characterized using Raman spectroscopy, field emission scanning electron microscopy (FE-SEM), energy dispersive spectroscopy (EDS), x-ray photoelectron spectroscopy (XPS), inductively coupled plasma (ICP), and transmission electron

microscopy (TEM). Cyclic voltammetry (CV) was employed to evaluate the catalytic properties of EPD Pt/GO/CP in half cell reactions.

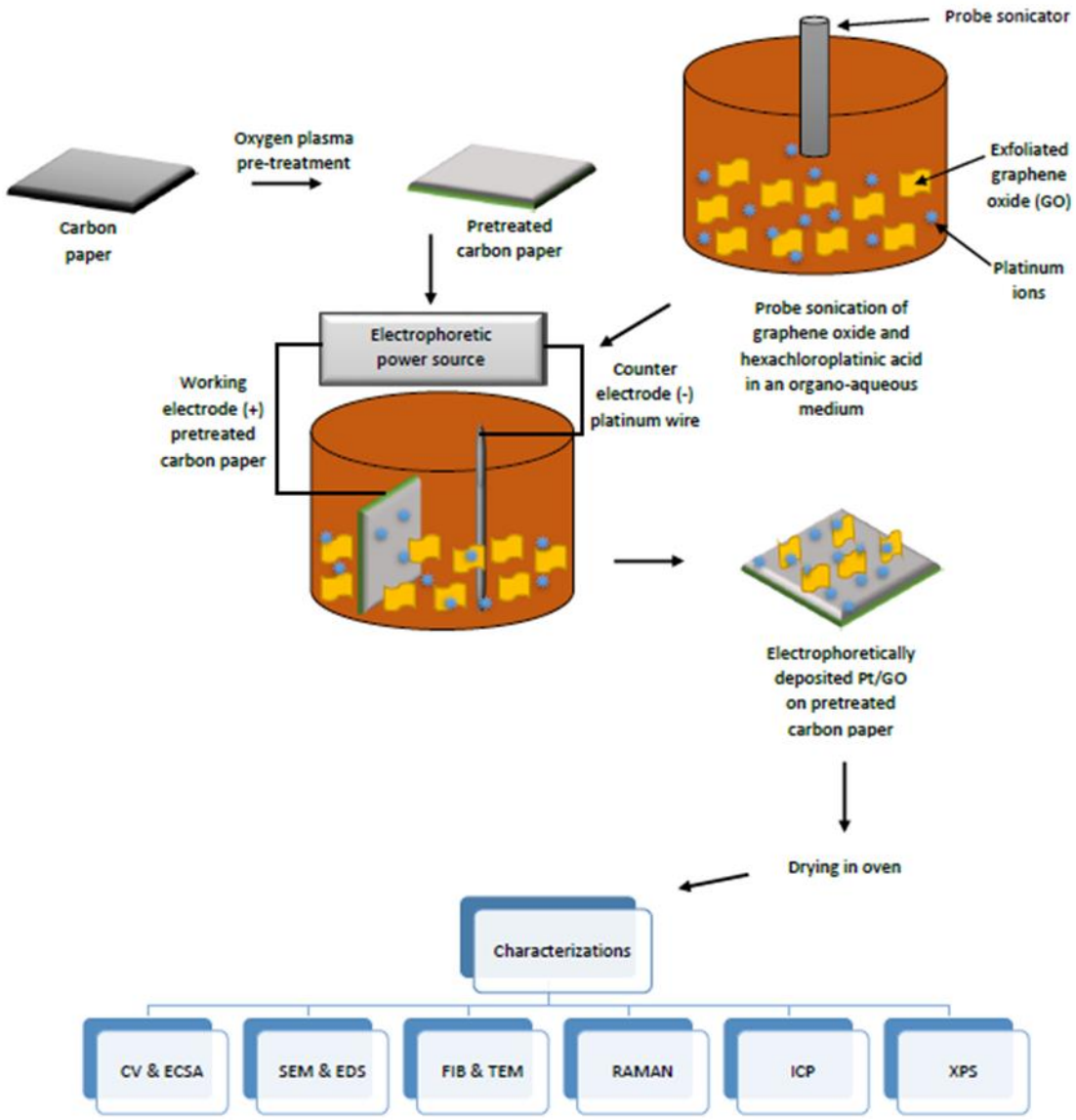

Figure 7. Schematic representation of the EPD process followed by characterization.

2. Experimental

2.1. Reagents and Chemicals

Following chemicals were used in this study: chloroplatinic acid hexahydrate (H_2PtCl_6 . $6H_2O$) or hexachloroplatinic acid (Sigma-Aldrich®), graphene oxide (GRAnPH Nanotech), AvCarb® MGL190 carbon paper (Fuel Cell Store), H_2SO_4 (Sigma-Aldrich®, 99.99%), ethanol (Sigma-Aldrich®, 99.8%), and deionized water.

2.2. Synthesis of Pt/GO Nanocomposites via EPD

The preparation of EPD colloidal solution involved following steps. The as obtained GO was probe sonicated (Q700 Sonicator, QSONICA, U.S.A.) in an ice bath for 20 minutes (GO concentration, 1.5 mg/mL of organo-aqueous solvent of 1:1 w/w ethanol:water). In the meantime, 0.05 M hexachloroplatinic acid (HCPA) in organo-aqueous solvent was magnetically stirred (MSH-20D Stirrer, Germany) for 20 minutes. The stirred HCPA solution was then poured into the GO solution and probe sonication was continued for another 20 minutes. The working electrode, AvCarb® MGL190 carbon paper, were cut into 2.5" x 2.5" dimensions and subjected to O_2 plasma pre-treatment (Torr Plasma Asher, U.S.A.) at 100 W/2 minutes. The EPD process was carried in a homemade glass electrochemical cell at room temperature (Figure 8).

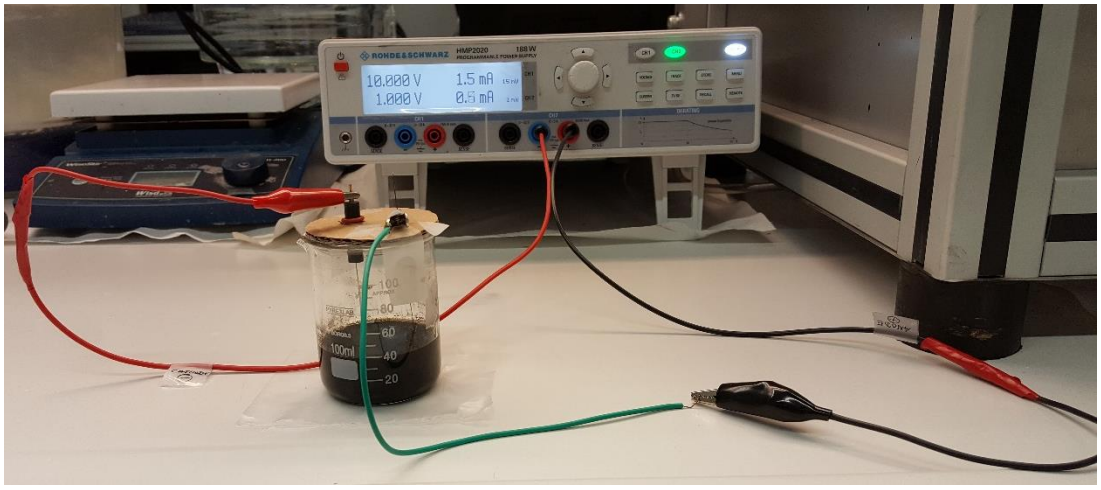

Figure 8. Homemade electrochemical cell.

The EPD was performed using two electrodes i.e. a working electrode (WE) connected to the anode source, and a counter electrode (CE) connected to the cathode source.

The WE were the O_2 plasma pre-treated carbon paper, while the CE was a Pt wire auxiliary electrode (MW-1032, BASi®, U.S.A.). The probe sonicated Pt/GO solution was used as an EPD electrolyte. The distance between the WE and CE was 1 cm. The electrodes were connected to a power supply (HMP2020, Rohde & Schwarz, U.S.A.). After optimizing EPD parameters, Pt nanoparticles and GO were deposited electrophoretically on carbon paper at 10 V for 80, 120, 240, and 300 minutes, respectively. After the EPD was completed, freshly prepared samples were dried out in an oven at 70°C/30 minutes.

2.3. Physical Characterization

Raman spectroscopy (Renishaw inVia™ Reflex Raman Microscope and Spectrometer; laser excitation at 532 nm) was used to study the electrophoretically deposited GO. FE-SEM (Supra Gemini 35 VP, Leo, ZEISS, Germany), focused ion beam (FIB), and TEM (Hitachi HT7700, Japan) were used to ascertain the size and morphology of Pt nanoparticles and GO on the catalyst layer. XPS (SPECS™ XP FlexMod, Germany) was used to study different oxidation states of Pt. ICP (Perkin Elmer ELAN DRC-e, U.S.A.) was employed to find out the mass of the deposited Pt nanoparticles. Elemental analysis of the samples was done via EDS.

2.4. Electrochemical Characterization

The obtained samples were electrochemically characterized by cyclic voltammetry (CV) (Gamry Reference 3000 Potentiostat/Galvanostat/ZRA, U.S.A.) using a 3-electrode setup which consisted of EPD Pt/GO/CP as working electrodes (WE), Ag/AgCl (MF-2052 RE-5B, BASi®, U.S.A.) as a reference electrode (RE), and Pt wire (MW-1032, BASi®, U.S.A.) as a counter electrode (CE). Prior to the beginning of electrochemical experiments, the electrolyte (20 mL 0.5 M H_2SO_4) in the electrode cell was de-aerated with N_2 for 30 minutes. CV was performed at a scan rate of 50 mV/s within the potential window of -0.2 to 1.0 V vs. Ag/AgCl at ambient conditions. The cyclic voltammograms were obtained after 20 cycle scans to attain stable current-potential behavior. The electrochemically active surface area (ECSA) was calculated by integrating the CV by taking the average between desorption and adsorption charges [18, 60].

3. Results and Discussion

The EPD of Pt nanoparticles from HCPA can be explained by the following equations (xiii, xiv, xv) [16]:

$$Pt^{4}Cl_6^{2-} + 2e^- \rightarrow Pt^{2}Cl_4^{2-} + 2Cl^- \quad \text{(xiii)}$$

$$Pt^{2}Cl_4^{2-} + 2e^- \rightarrow Pt + 4Cl^- \quad \text{(xiv)}$$

$$Pt^{4}Cl_6^{2-} + 4e^- \rightarrow Pt + 6Cl^- \quad \text{(xv)}$$

EPD of Pt nanoparticles can follow two paths. Either Pt nanoparticles are EPD via two steps (equations xiii and xiv) by gaining 2 electrons in each step or by a single step (equation xv) by gaining 4 electrons with the evolution of chlorine gas in each case.

3.1. Morphology

Figures 9 - 12 show the SEM micrographs of the obtained Pt/GO nanocomposites electrophoretically deposited onto carbon paper at 10 V for 80, 120, 240, and 300 minutes, respectively. Through SEM, it was observed that the deposition of exfoliated GO was a direct function of higher EPD time. As the EPD time increased from 80 to 300 minutes, more overlapped GO flakes with wrinkled morphology were deposited onto the carbon paper. In figures 10 - 12, conglomerated small sized GO flakes (appearing as white deposits) are seen to be spread throughout the entire matrix of carbon paper fibers which is probably due to more exfoliation time of GO during probe sonication.

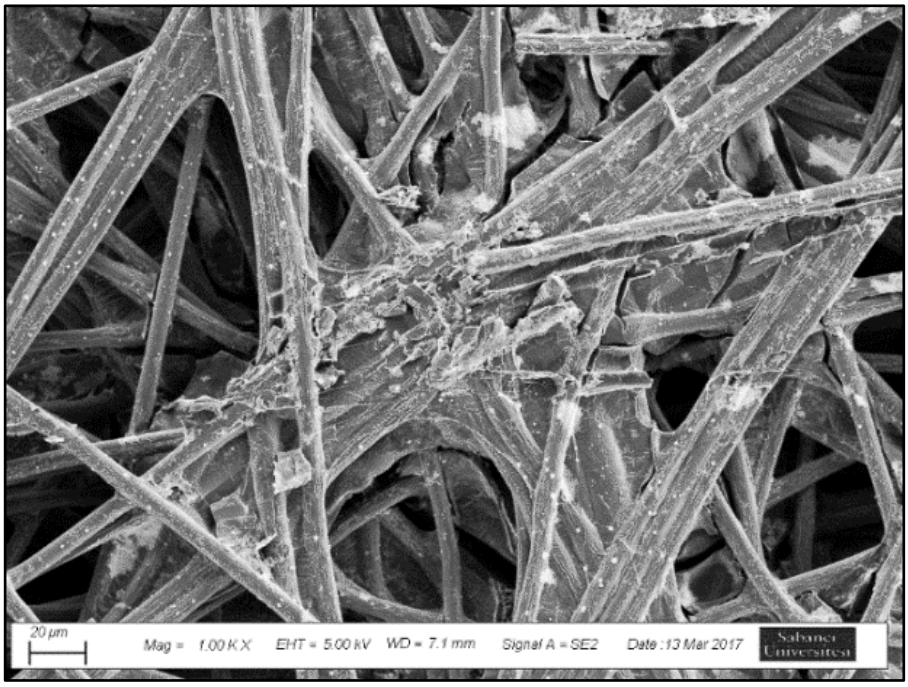

Figure 9. SEM micrograph of Pt/GO/CP electrophoretically deposited at 10 V/80 minutes.

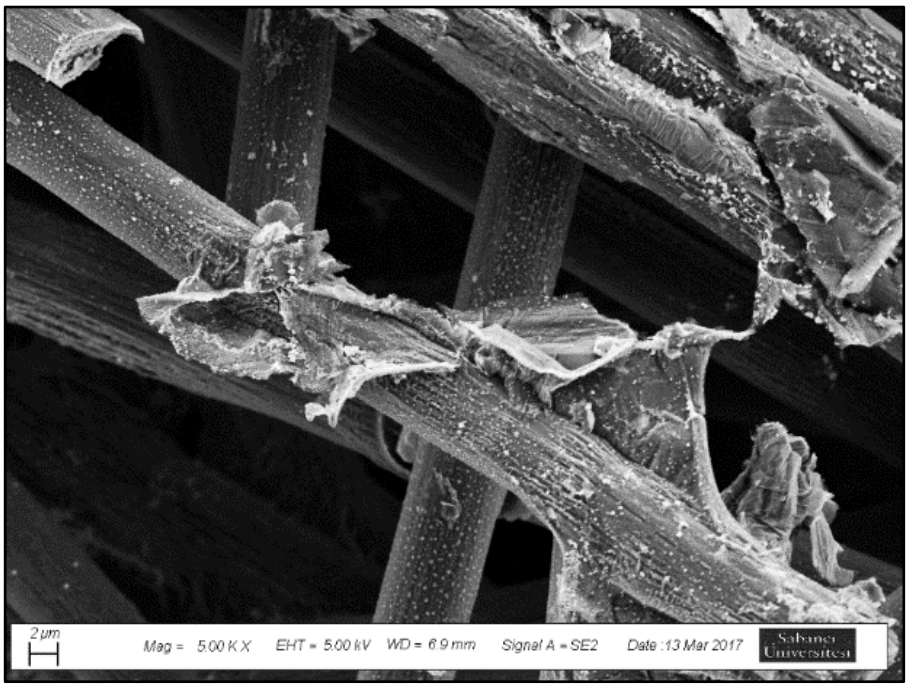

Figure 10. SEM micrograph of Pt/GO/CP electrophoretically deposited at 10 V/120 minutes.

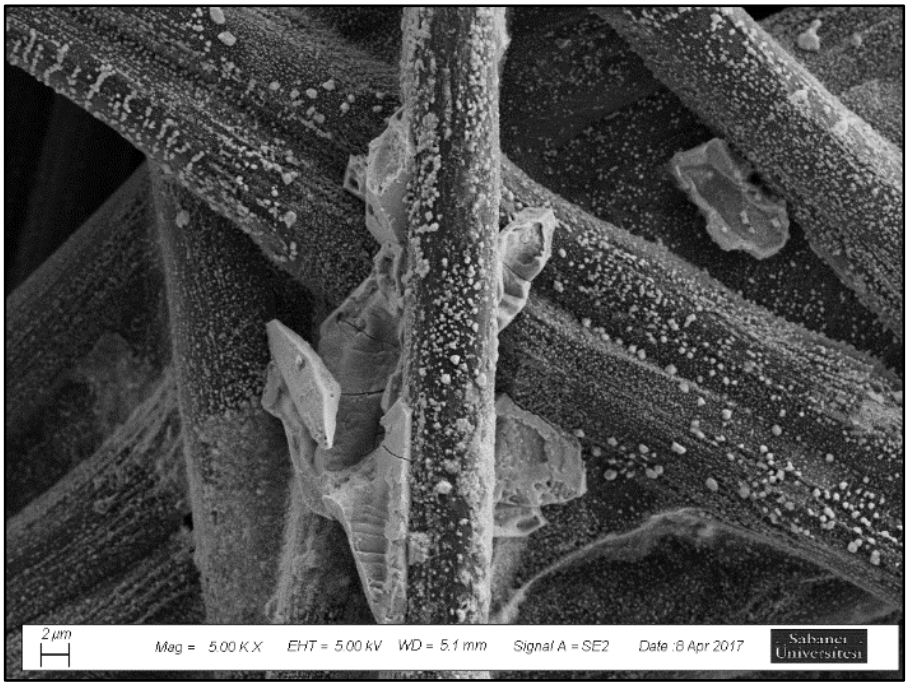

Figure 11. SEM micrograph of Pt/GO/CP electrophoretically deposited at 10 V/240 minutes.

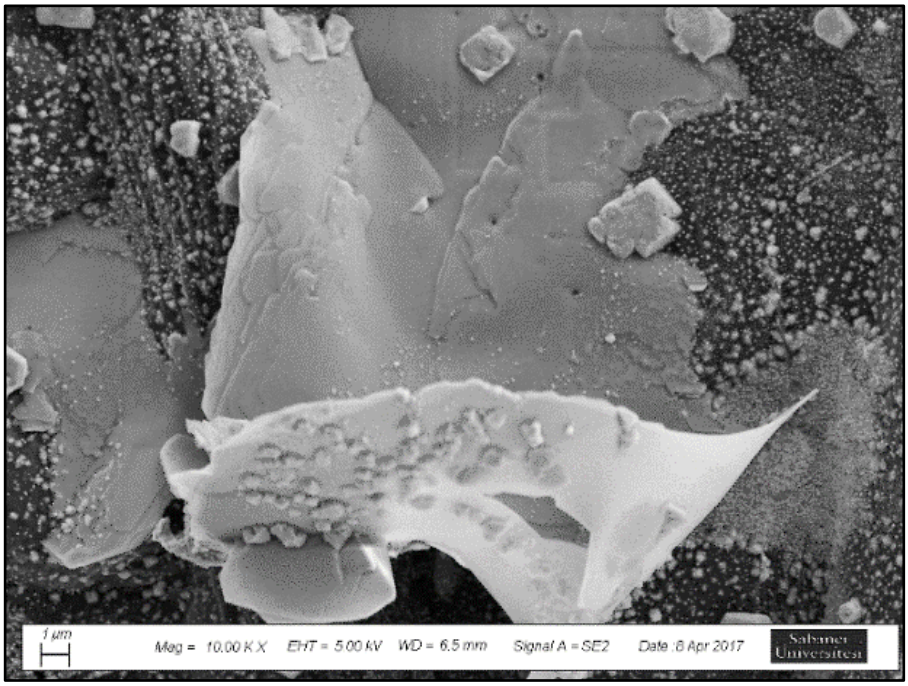

Figure 12. SEM micrograph of Pt/GO/CP electrophoretically deposited at 10 V/300 minutes.

3.2. Elemental Analysis

Pt/GO/CP electrophoretically deposited at 10 V for 80, 120, 240, and 300 minutes, were analyzed via backscattered electron imaging and EDS. The EDS spectra shows peaks related to C and Pt elements, corroborating the deposition of Pt nanoparticles on GO and carbon substrate. Furthermore, by employing EDS elemental mapping, it was observed that the atomic percentage of the deposited Pt on all the samples was almost the same i.e. 0.2 ~ 0.3% (Figure 13).

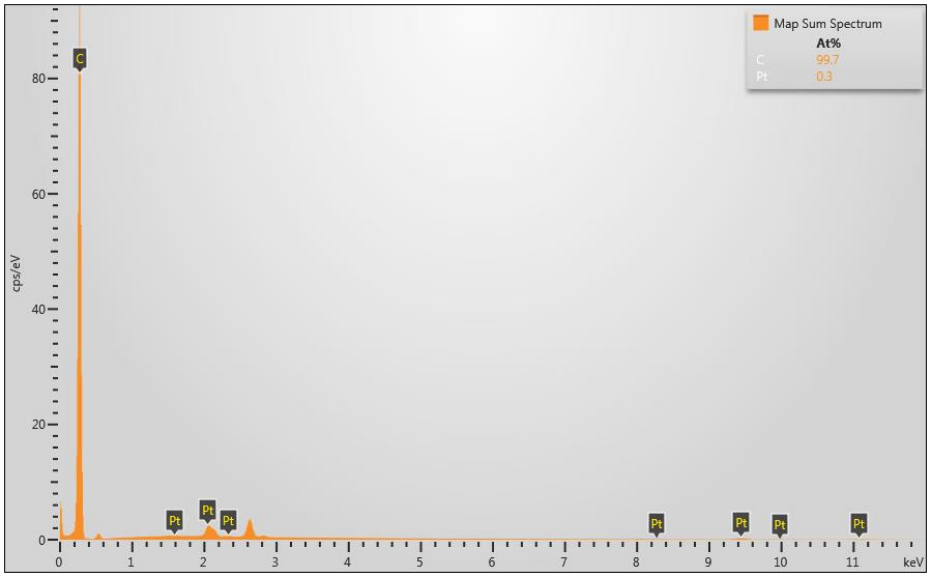

Figure 13. EDS spectra of Pt/GO/CP electrophoretically deposited at 10 V/240 minutes.

3.3. Morphology (TEM)

The TEM specimens were prepared using FIB. TEM images were obtained at 120 kV. Figures 14 and 15 represent TEM images of Pt nanoparticles followed by their corresponding particle size distribution histograms. It can be seen in the images that Pt nanoparticles are uniformly deposited and are attached onto the surface and interspaces of single and multilayers of GO. The average Pt particle size is determined to be about 5.8 ~ 6.0 nm. These nanoparticles augmented the electrochemical activity which was observed during the ECSA. Furthermore, with the help of XPS analysis it was observed that not all the deposited Pt is in its metallic state, rather Pt has been found to be oxidized as PtO and PtO_2 which is plausible due to Pt interaction with the functional groups present on GO surface [81].

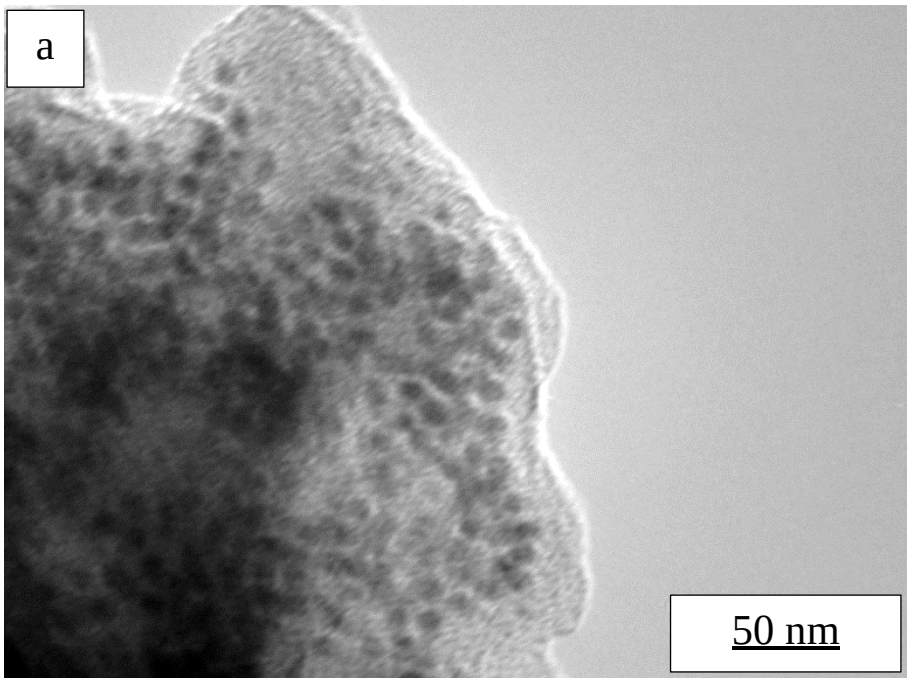

Figure 14. TEM image of Pt nanoparticles EPD on GO sheets at 10 V/120 minutes.

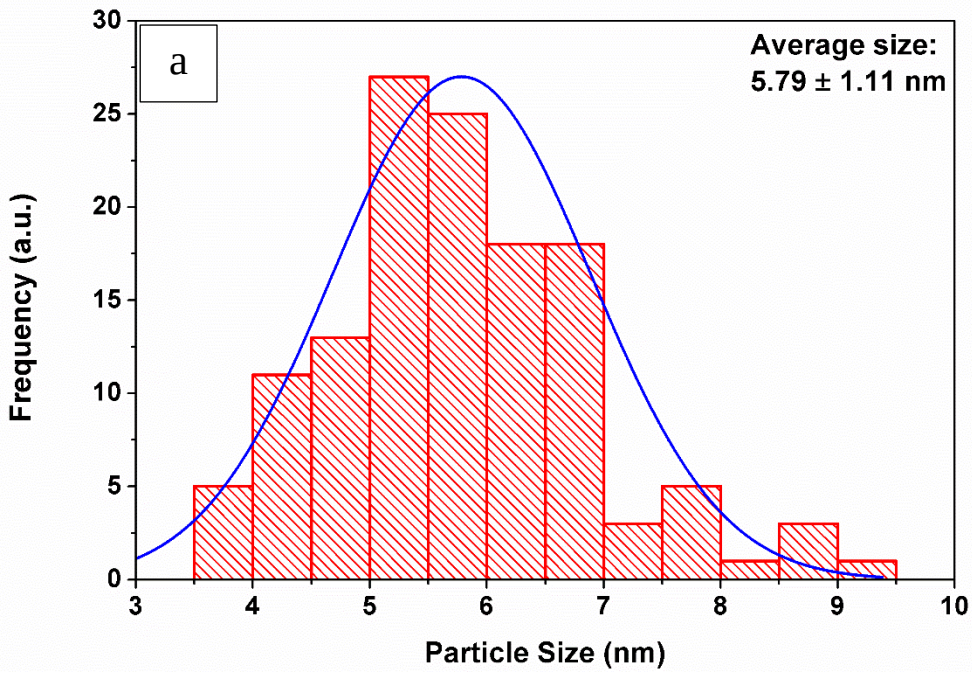

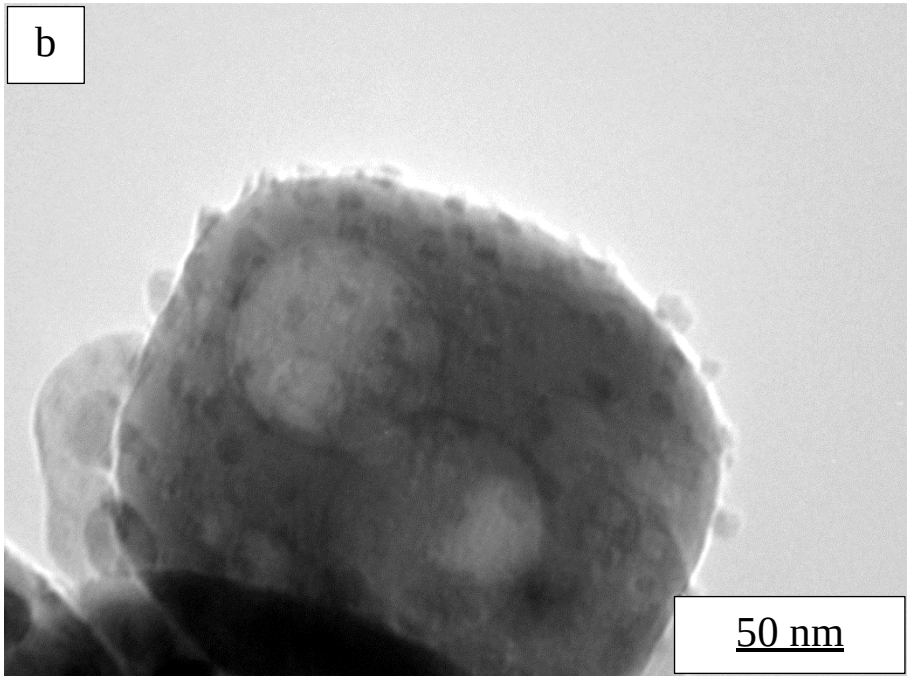

Figure 15. TEM image of Pt nanoparticles EPD on GO sheets at 10 V/240 minutes.

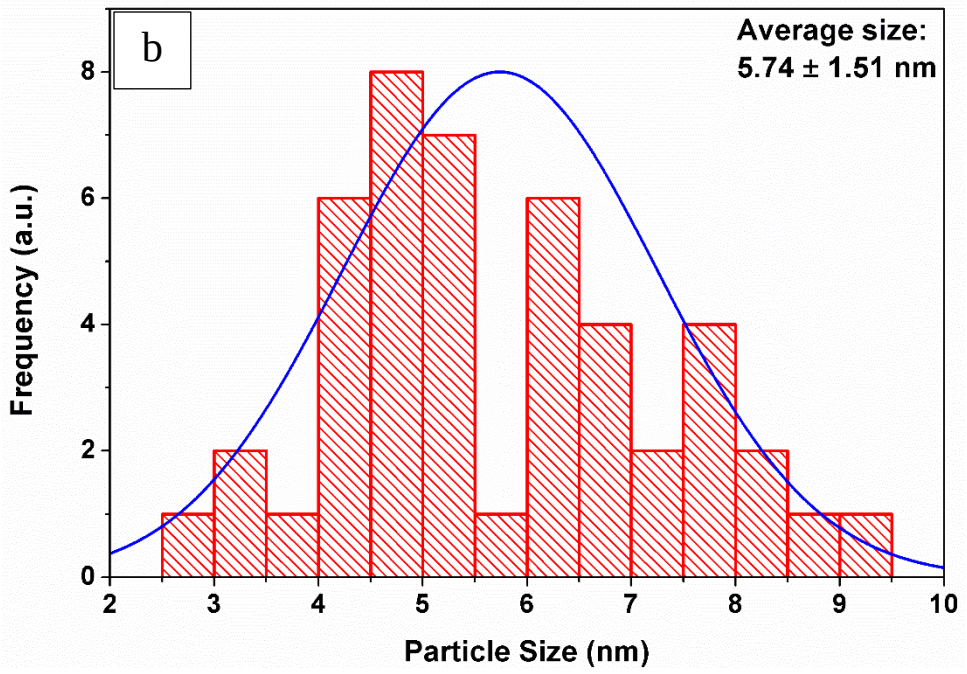

3.4. Electrochemical Characterization (CV and ECSA)

Different methods can be used to determine active catalytic surface sites [82]. Among these methods, CV, for decades has been employed to evaluate the catalyst utilization and ECSA of fuel cell electrocatalysts. Catalyst utilization and ECSA are benchmarks for developers to assess the performance of catalysts and MEA [59]. During CV, the WE is cycled through a potential voltage window to achieve H^+ adsorption and desorption data necessary for calculating ECSA [59, 82]. The ECSA of an electrocatalyst gives information pertaining to the number of electrochemically active sites per gram of catalyst [31, 46, 72, 82]. It is calculated by integrating hydrogen adsorption and desorption peaks after subtracting the double layer region [72]. In this research, for ECSA, we took the average between anodic desorption and cathodic adsorption charges as it has been previously employed in the literature [18, 60]. The hydrogen desorption/adsorption reactions are as follows [59]:

$$Pt - H_{ads} \rightarrow Pt + H^+ + e^- \qquad \text{(Anodic/forward scan)}$$

$$Pt + H^+ + e^- \rightarrow Pt - H_{ads} \qquad \text{(Cathodic/reverse scan)}$$

The above reactions are based on two assumptions. First, each H^+ can occupy one site on the available Pt surface. Second, all the active and accessible sites will be filled by hydrogen atom during the transition from H^+ adsorption to H_2 evolution and vice versa. Therefore, the total number of moles of charge passed during H^+ adsorption/desorption is assumed to be equal to the number of moles of active sites [82]. Figure 16 presents the cyclic voltammograms of EPD Pt/GO/CP in N_2-saturated 0.5 M H_2SO_4 electrolyte at a scan rate of 50 mV/s.

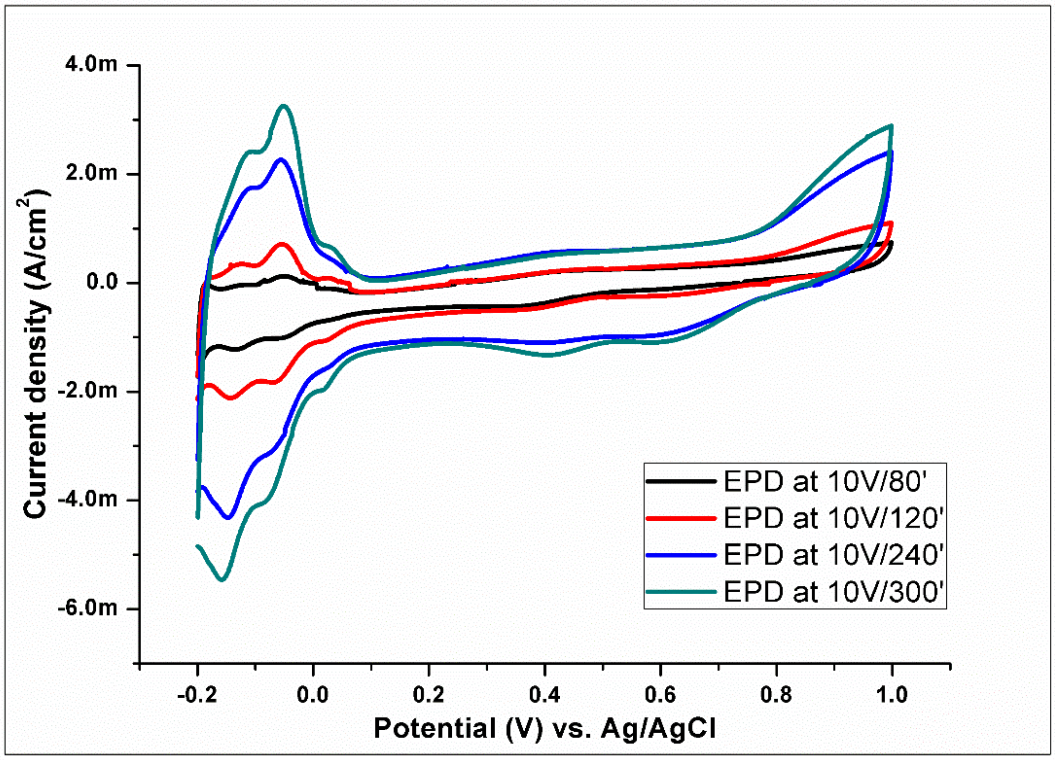

Figure 16. Cyclic voltammograms of EPD Pt/GO/CP in N_2-saturated 0.5 M H_2SO_4 electrolyte at a scan rate of 50 mV/s.

The ECSA of the Pt catalyst was calculated using the following expression [31, 72]:

$$\text{ECSA}\ [\text{cm}^2\ \text{Pt/g of Pt}] = \frac{\text{charge}\ [\text{Q}_\text{H}, \mu\text{C/cm}^2]}{210\ [\mu\text{C/cm}^2] \times \text{electrode loading}\ [\text{g of Pt/cm}^2]}$$

In the given expression, Q_H is the charge density which is calculated by integrating the cyclic voltammograms; 210 $\mu C/cm^2$ is charge needed to reduce a monolayer of H^+ on polycrystalline Pt [18, 59, 60, 73]; and electrode loading is the mass of Pt electrophoretically deposited on the WE [73], which was determined by using ICP. The ECSA for the Pt/GO/CP were computed using above-mentioned equation and results are shown in Table 1.

Table 1. ECSA for electrophoretically deposited Pt/GO nanocomposites

EPD Pt/GO/CP	Q_H (mC/cm^2)	Pt loading (µg/cm^2)	ECSA (m^2/g)
10 V/80 minutes	1.15	68	8
10 V/120 minutes	3.00	161	9
10 V/240 minutes	7.43	129	27
10 V/300 minutes	10.26	312	16

From Table 1, it can be noticed that with an increment in EPD time, there is an increase in Pt loading, and hence an increase in ECSA values is observed (deposition at 80 and 120 minutes). But at higher deposition time i.e. 240 and 300 minutes, the results deviated. At 300 minutes deposition, Pt loading is higher than rest of the samples, contrarily the ECSA value is lesser than 240 minutes' deposited Pt/GO nanocomposites' ECSA value. This trend has been observed by Taylor *et al.* [22] who reported that the plausible cause for this decrement in ECSA value is linked to Pt particle agglomeration at higher Pt loadings, which eventually weakens the overall activity of Pt surface area [18, 22]. The highest ECSA value of 27.41 m^2/g was achieved at an optimized Pt loading of 0.129 mg/cm^2 which is close to the 2017 target value set by the U.S. Department of Energy (≤ 0.125 mg/cm^2) [58]. These results can be ascribed to the dispersion of Pt nanoparticles on GO nano sheets displaying synergetic performance as catalyst necessary for PEMFC.

Figure 16 displays four cyclic voltammograms of Pt/GO/CP electrophoretically deposited at 10 V for 80, 120, 240, and 300 minutes, respectively. Following are the general features that are common to all the curves:

I. In the cathodic scan, hydrogen adsorption/evolution occurred from ~0.05 to –0.2 V vs. Ag/AgCl RE. During this negative scan, hydrogen adsorption onto the Pt surface augmented as the EPD time was increased. And it is evident from the CV curves that higher Pt loadings lead to better hydrogen adsorption followed by hydrogen evolution.

II. In the anodic scan, hydrogen desorption/oxidation occurred at around the same voltage range as hydrogen adsorption/evolution. During this scan, owing to the increased EPD time which lead to higher Pt deposition, hydrogen desorption peaks were amplified. The process is fast and electrochemically reversible and thus it is possible that some of the hydrogen evolved during the reverse scan might reoxidize [82].

3.5. XPS characterization

Figure 17 presents Pt 4f XPS spectra for Pt/GO/CP (chosen sample EPD at 10 V/240 minutes). Pt 4f of the selected sample displayed the "expected doublets" and the signal is deconvoluted into two components, Pt $4f_{7/2}$ and Pt $4f_{5/2}$, with Pt of 0, +II, and +IV oxidation states [26]. Due to the baseline correction, there is a slight shift in the deconvoluted peaks of the respective Pt $4f_{7/2}$ and Pt $4f_{5/2}$. The peaks corresponding to the Pt $4f_{7/2}$ located at 71.4, 72.0, and 73.0 eV are assigned to metallic Pt^0, Pt^{+II}, and Pt^{+IV}, respectively. Contrarily, the peaks corresponding to the Pt $4f_{5/2}$ located at 74.7, 75.4, and 78.0 eV are assigned to metallic Pt^0, Pt^{+II}, and Pt^{+IV}, respectively. The presence of Pt^{+II} or Pt^{+IV} could be linked to partial or complete oxidation of Pt^0 on the GO surface [81].

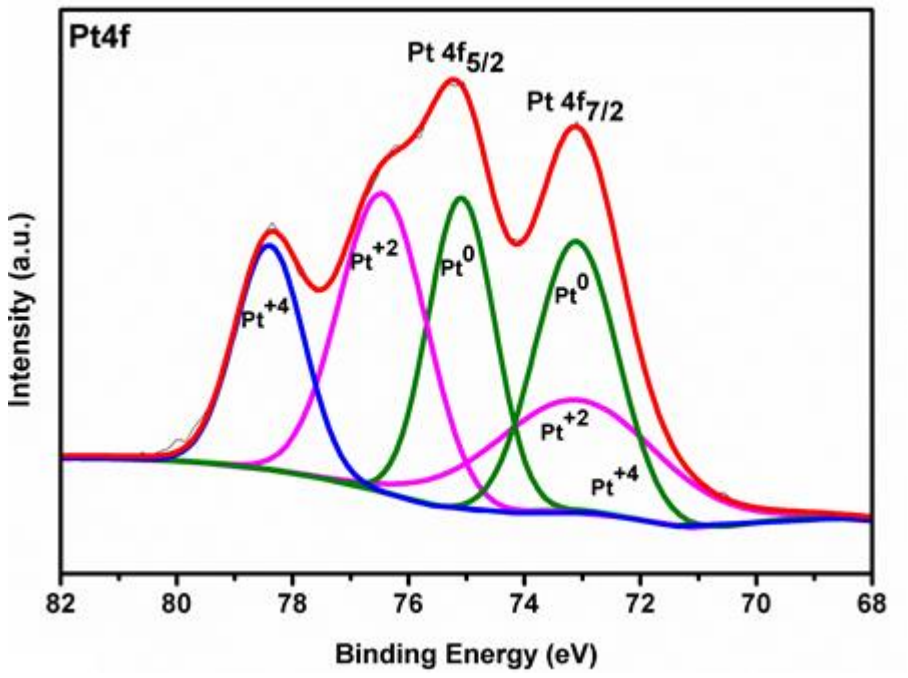

Figure 17. XPS spectra of Pt 4f for Pt/GO/CP.

3.6. Structure (Raman Spectroscopy)

Raman spectroscopy is a well-established noninvasive tool used to study allotrope, crystalline, nanocrystalline, and amorphous carbon [51, 83]. In the literature, Raman spectroscopy has been employed in studying the crystal structure, defects, and disorders in graphene and graphene related materials [47, 50, 84]. In this spectroscopy, a monochromatic laser (wavelength of 532 nm) interacts with the vibrational modes and phonons in the specimen, causing to shift the "Stokes and anti-Stokes" via inelastic scattering [47, 83]. In graphene Raman spectrum, there are four common types of defect peaks: D (1350 cm^{-1}), G (1580 cm^{-1}), D' (1620 cm^{-1}), and 2D (2690 cm^{-1}) [47, 51]. D and 2D peaks are laser excitation dependent peaks, also known as second order overtone of different in-plane vibrations. On the other hand, G peaks are the primary in-plane vibrational modes. The D peak does not occur in pristine graphene [83] because of crystal symmetries. But as the disorders in graphene increase, Raman intensity increases for the three distinct disorder peaks i.e. D, D', and D+G (2940 cm^{-1}), respectively [47]. The level of disorder in graphene can be studied from the ratio of the D and G peaks (I_D/I_G) [47, 51, 84].

Figure 18 represents the Raman spectrum of EPD Pt/GO nanocomposites over a fixed voltage (10 V) at different deposition time i.e. 80, 120, 240, and 300 minutes. The two prominent peaks were D and G, occurring at ~1351 cm^{-1} and ~1582 cm^{-1}, respectively. With an increase in deposition time, the intensity of D peaks for all the samples increased, while the intensity of G peaks remained marginally steady. The D peaks have breathing mode A_{1g} symmetry [83] and are induced because of in-plane edges and grain boundaries of graphene crystals. The hexagonal crystal lattice of graphene has two types of crystal edges, namely, armchair and zigzag. It is because of these armchair edges that the charge carriers are inelastically scattered by the phonons and excited, followed by an elastic scattering near the K zone boundary leading to the prominence of D peaks in graphene [47, 83]. On the contrary, the G peaks have an E_{2g} symmetry and arise from an "in-plane bond-stretching motion of carbon sp^2 atoms". Also, these peaks are independent of sixfold rings, and therefore occur at all sp^2 sites [83]. Hence, these peaks show the presence of crystalline graphene layers [55]. The intensity ratio of the D and G peaks for the EPD Pt/GO nanocomposites at 80, 120, 240, and 300 minutes were found to be 0.25, 0.54, 0.88, and 0.79, respectively (Table 2). The decrement in the I_D/I_G value at 80 minutes electrodeposition is an indication of better defect

repairs [85]. In other words, increase in defect density indicates the presence of more sp^2 amorphous carbon structure [47, 51]. The increment in the I_D/I_G values at higher electrodeposition time i.e. 120, 240, and 300 minutes, is justified by the fact that at low defect density more elastic scattering occurs which indicates the presence of "nanocrystalline graphene phase" [47].

Table 2. Raman shift positions and I_D/I_G values for EPD Pt/GO nanocomposites

EPD Pt/GO/CP	D peak (cm^{-1})	G peak (cm^{-1})	I_D/I_G
10 V/80 minutes	1347	1580	0.25
10 V/120 minutes	1354	1580	0.54
10 V/240 minutes	1352	1583	0.88
10 V/300 minutes	1349	1583	0.79

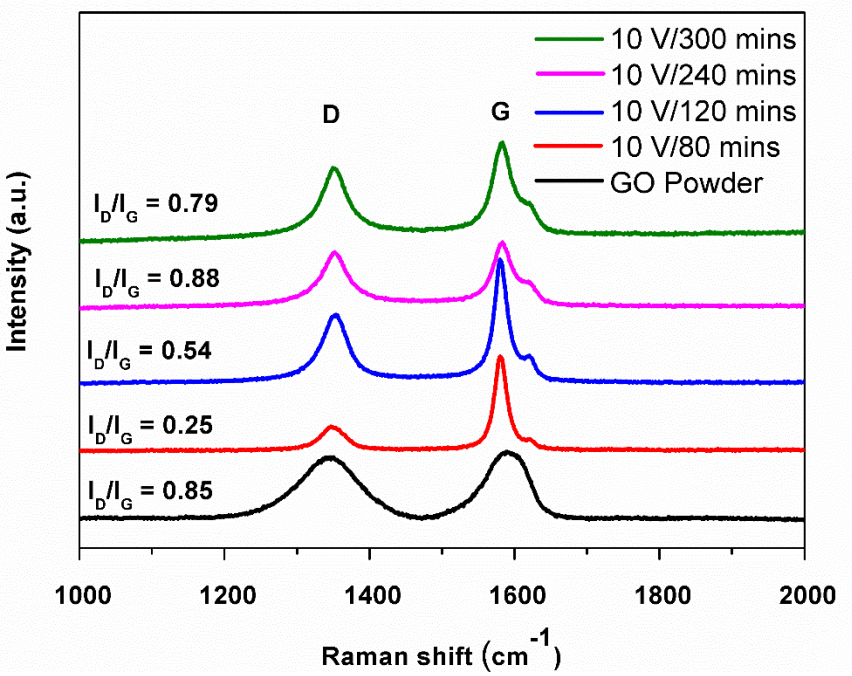

Figure 18. Raman spectrum of EPD Pt/GO nanocomposites obtained at different deposition time.

4. Conclusions

EPD, an eco-friendly, simple and fast method has been adopted for the synthesis of Pt/GO nanocomposites as catalyst for PEMFC. During this work, it was found that using a mixture of organic and aqueous solvent was ideal for better dispersion and stability of GO and Pt in the EPD solution. After optimizing the parameters, best results were obtained at deposition of 10 V/80, 120, 240, and 300 minutes, respectively. The incorporation of GO's 2D structure ranging from mono to few layers in the catalyst matrix helped in better anchoring of Pt onto the carbon paper surface and GO surface. ECSA value decreased at higher Pt loading (10 V/300 minutes) which is possible due to the clustering of Pt nanoparticles. Further work requires an in-situ evaluation of the developed Pt/GO/CP in a single fuel cell necessary to determine their ORR activity and power output.

5. References

1. Hamilton PJ, Pollet BG. Polymer Electrolyte Membrane Fuel Cell (PEMFC) Flow Field Plate: Design, Materials and Characterisation. Fuel Cells. 2010;10(4):489-509.
2. Lin Z, Ji L, Zhang X. Electrodeposition of platinum nanoparticles onto carbon nanofibers for electrocatalytic oxidation of methanol. Materials Letters. 2009;63(24-25):2115-8.
3. Salernitano E, Giorgi L, Dikonimos Makris T. Direct growth of carbon nanofibers on carbon-based substrates as integrated gas diffusion and catalyst layer for polymer electrolyte fuel cells. International Journal of Hydrogen Energy. 2014;39(27):15005-16.
4. Cambridge Uo. Fuel Cells 2017 [Available from: http://www.ceb.cam.ac.uk/research/groups/rg-eme/teaching-notes/fuelcells.
5. Matthey J. History of Fuel Cells: www.fuelcelltoday.com; 2017 [Available from: http://www.fuelcelltoday.com/history.
6. Quesnel E, Roux F, Emieux F, Faucherand P, Kymakis E, Volonakis G, et al. Graphene-based technologies for energy applications, challenges and perspectives. 2D Materials. 2015;2(3):030204.
7. DOE US. Types of Fuel Cells 2017 [Available from: https://energy.gov/eere/fuelcells/types-fuel-cells.
8. Singh V, Joung D, Zhai L, Das S, Khondaker SI, Seal S. Graphene based materials: Past, present and future. Progress in Materials Science. 2011;56(8):1178-271.
9. Meier JC, Galeano C, Katsounaros I, Witte J, Bongard HJ, Topalov AA, et al. Design criteria for stable Pt/C fuel cell catalysts. Beilstein J Nanotechnol. 2014;5:44-67.
10. Morikawa H, Tsuihiji N, Mitsui T, Kanamura K. Preparation of Membrane Electrode Assembly for Fuel Cell by Using Electrophoretic Deposition Process. Journal of The Electrochemical Society. 2004;151(10):A1733.
11. FuelCells.org. Types of Fuel Cells 2017 [Available from: http://hfcarchive.org/fuelcells/base.cgim?template=types_of_fuel_cells.

12. Rao C, Trivedi D. Chemical and electrochemical depositions of platinum group metals and their applications. Coordination Chemistry Reviews. 2005;249(5-6):613-31.
13. Larminie J, Dicks A, McDonald MS. Fuel cell systems explained: J. Wiley Chichester, UK; 2003.
14. Munakata H, Ishida T, Kanamura K. Electrophoretic Deposition for Nanostructural Design of Catalyst Layers on Nafion Membrane. Journal of The Electrochemical Society. 2007;154(12):B1368.
15. Binninger T, Fabbri E, Kötz R, Schmidt T. Determination of the electrochemically active surface area of metal-oxide supported platinum catalyst. Journal of The Electrochemical Society. 2014;161(3):H121-H8.
16. Saminathan K, Kamavaram V, Veedu V, Kannan AM. Preparation and evaluation of electrodeposited platinum nanoparticles on in situ carbon nanotubes grown carbon paper for proton exchange membrane fuel cells. International Journal of Hydrogen Energy. 2009;34(9):3838-44.
17. Wee J-H, Lee K-Y, Kim SH. Fabrication methods for low-Pt-loading electrocatalysts in proton exchange membrane fuel cell systems. Journal of Power Sources. 2007;165(2):667-77.
18. Pozio A, De Francesco M, Cemmi A, Cardellini F, Giorgi L. Comparison of high surface Pt/C catalysts by cyclic voltammetry. Journal of power sources. 2002;105(1):13-9.
19. Holton OT, Stevenson JW. The Role of Platinum in Proton Exchange Membrane Fuel Cells. Platinum Metals Review. 2013;57(4):259-71.
20. Cambridge Uo. Types of Fuel Cells 2017 [Available from: http://www.ceb.cam.ac.uk/research/groups/rg-eme/teaching-notes/fuelcells/types-of-fuel-cells.
21. Rost U, Marginean G, Muntean R, Podleschny P, Brodmann M, Merino C, et al., editors. A cost-effective PEM fuel cell test system based on hydraulic compression with optimized platinum catalyst loading. Energy and Sustainability Conference (IESC), 2016 International; 2016: IEEE.

22. Taylor S, Fabbri E, Levecque P, Schmidt TJ, Conrad O. The Effect of Platinum Loading and Surface Morphology on Oxygen Reduction Activity. Electrocatalysis. 2016;7(4):287-96.
23. Adilbish G, Lee J-W, Jang Y-S, Lee H-G, Yu Y-T. Preparation of Pt/C electrode with double catalyst layers by electrophoresis deposition method for PEMFC. International Journal of Hydrogen Energy. 2014;39(7):3381-6.
24. Weiser M, Schulze C, Schneider M, Michaelis A. Platinum electrodeposition from a dinitrosulfatoplatinate(II) electrolyte. Applied Surface Science. 2016;390:333-8.
25. Louh RF, Huang H, Tsai F. Novel Deposition of Pt/C Nanocatalysts and Nafion® Solution on Carbon-Based Electrodes via Electrophoretic Process for PEM Fuel Cells. Journal of Fuel Cell Science and Technology. 2007;4(1):72.
26. Coutanceau C, Baranton S, Napporn T. Platinum Fuel cell nanoparticle syntheses: effect on morphology, structure and electrocatalytic behavior. The Delivery of Nanoparticles: InTech; 2012.
27. Brownson DAC, Kampouris DK, Banks CE. An overview of graphene in energy production and storage applications. Journal of Power Sources. 2011;196(11):4873-85.
28. Taylor E, Anderson E, Vilambi N. Preparation of High-Platinum-Utilization Gas Diffusion Electrodes for Proton-Exchange-Membrane Fuel Cells. Journal of the Electrochemical Society. 1992;139(5):L45-L6.
29. Islam MA, Islam MS. Electro-deposition Method for Platinum Nano-particles Synthesis. Engineering International. 2013;1(2):9-17.
30. Domínguez-Domínguez S, Arias-Pardilla J, Berenguer-Murcia Á, Morallón E, Cazorla-Amorós D. Electrochemical deposition of platinum nanoparticles on different carbon supports and conducting polymers. Journal of Applied Electrochemistry. 2007;38(2):259-68.
31. Seger B, Kamat PV. Electrocatalytically active graphene-platinum nanocomposites. Role of 2-D carbon support in PEM fuel cells. The Journal of Physical Chemistry C. 2009;113(19):7990-5.
32. Yao Z, Yue R, Zhai C, Jiang F, Wang H, Du Y, et al. Electrochemical layer-by-layer fabrication of a novel three-dimensional Pt/graphene/carbon fiber electrode

and its improved catalytic performance for methanol electrooxidation in alkaline medium. International Journal of Hydrogen Energy. 2013;38(15):6368-76.

33. Maiyalagan T, Dong X, Chen P, Wang X. Electrodeposited Pt on three-dimensional interconnected graphene as a free-standing electrode for fuel cell application. Journal of Materials Chemistry. 2012;22(12):5286.

34. Wang Q, Wang Q, Li M, Szunerits S, Boukherroub R. Preparation of reduced graphene oxide/Cu nanoparticle composites through electrophoretic deposition: application for nonenzymatic glucose sensing. RSC Adv. 2015;5(21):15861-9.

35. Diba M, Boccaccini A. Electrophoretic Deposition of Graphene-Based Materials and Their Energy-Related Applications. 2016:173-86.

36. Zhou YG, Chen JJ, Wang FB, Sheng ZH, Xia XH. A facile approach to the synthesis of highly electroactive Pt nanoparticles on graphene as an anode catalyst for direct methanol fuel cells. Chem Commun (Camb). 2010;46(32):5951-3.

37. Novoselov KS, Fal′ko VI, Colombo L, Gellert PR, Schwab MG, Kim K. A roadmap for graphene. Nature. 2012;490(7419):192-200.

38. Graphenea. Graphene Oxide - What Is It? 2017 [Available from: https://www.graphenea.com/pages/graphene-oxide#.WXUFF4iGPIU.

39. Lee W, Lee JU, Cha H-J, Byun J-H. Partially reduced graphene oxide as a multi-functional sizing agent for carbon fiber composites by electrophoretic deposition. RSC Advances. 2013;3(48):25609.

40. Yin PT, Shah S, Chhowalla M, Lee KB. Design, synthesis, and characterization of graphene-nanoparticle hybrid materials for bioapplications. Chem Rev. 2015;115(7):2483-531.

41. Ovid'ko I. Mechanical properties of graphene. Rev Adv Mater Sci. 2013;34(1):1-11.

42. Chartarrayawadee W, Moulton SE, Li D, Too CO, Wallace GG. Novel composite graphene/platinum electro-catalytic electrodes prepared by electrophoretic deposition from colloidal solutions. Electrochimica Acta. 2012;60:213-23.

43. Chavez-Valdez A, Shaffer MS, Boccaccini AR. Applications of graphene electrophoretic deposition. A review. J Phys Chem B. 2013;117(6):1502-15.

44. Zhao Y-Q, Zhao D-D, Tang P-Y, Wang Y-M, Xu C-L, Li H-L. MnO2/graphene/nickel foam composite as high performance supercapacitor

electrode via a facile electrochemical deposition strategy. Materials Letters. 2012;76:127-30.

45. Wu Z-S, Pei S, Ren W, Tang D, Gao L, Liu B, et al. Field Emission of Single-Layer Graphene Films Prepared by Electrophoretic Deposition. Advanced Materials. 2009;21(17):1756-60.

46. Qiu J-D, Wang G-C, Liang R-P, Xia X-H, Yu H-W. Controllable Deposition of Platinum Nanoparticles on Graphene As an Electrocatalyst for Direct Methanol Fuel Cells. The Journal of Physical Chemistry C. 2011;115(31):15639-45.

47. Childres I, Jauregui LA, Park W, Cao H, Chen YP. Raman spectroscopy of graphene and related materials. New developments in photon and materials research. 2013;1.

48. Cao G. Atomistic Studies of Mechanical Properties of Graphene. Polymers. 2014;6(9):2404-32.

49. Liu S, Wang J, Zeng J, Ou J, Li Z, Liu X, et al. “Green” electrochemical synthesis of Pt/graphene sheet nanocomposite film and its electrocatalytic property. Journal of Power Sources. 2010;195(15):4628-33.

50. Claramunt S, Varea A, López-Díaz D, Velázquez MM, Cornet A, Cirera A. The Importance of Interbands on the Interpretation of the Raman Spectrum of Graphene Oxide. The Journal of Physical Chemistry C. 2015;119(18):10123-9.

51. Grimm S, Schweiger M, Eigler S, Zaumseil J. High-Quality Reduced Graphene Oxide by CVD-Assisted Annealing. The Journal of Physical Chemistry C. 2016;120(5):3036-41.

52. Diba M, Fam DWH, Boccaccini AR, Shaffer MSP. Electrophoretic deposition of graphene-related materials: A review of the fundamentals. Progress in Materials Science. 2016;82:83-117.

53. García-Gómez A, Duarte RG, Eugénio S, Silva TM, Carmezim MJ, Montemor MF. Fabrication of electrochemically reduced graphene oxide/cobalt oxide composite for charge storage electrodes. Journal of Electroanalytical Chemistry. 2015;755:151-7.

54. Liu S, Ou J, Wang J, Liu X, Yang S. A simple two-step electrochemical synthesis of graphene sheets film on the ITO electrode as supercapacitors. Journal of Applied Electrochemistry. 2011;41(7):881-4.

55. Hassan S, Suzuki M, El-Moneim AA. Facile synthesis of MnO2/graphene electrode by two-steps electrodeposition for energy storage application. Int J Electrochem Sci. 2014;9:8340-54.
56. Wu M-S, Lin Y-P, Lin C-H, Lee J-T. Formation of nano-scaled crevices and spacers in NiO-attached graphene oxidenanosheets for supercapacitors. J Mater Chem. 2012;22(6):2442-8.
57. Shi J, Li X-S, Hu Y-Q, Hua Y-X. Electro-deposition of platinum nanoparticles on 4-mercaptobenzene-functionalized multi-walled carbon nanotubes. Journal of Solid State Electrochemistry. 2008;12(12):1555-9.
58. Garland NL. DOE's fuel cell catalyst R&D activities. Arlington, VA, U.S.A.2012.
59. Cooper KR. In situ PEM fuel cell electrochemical surface area and catalyst utilization measurement. Fuel Cell Magazine. 2009;9.
60. Łukaszewski M. Electrochemical Methods of Real Surface Area Determination of Noble Metal Electrodes – an Overview. International Journal of Electrochemical Science. 2016:4442-69.
61. Bhowmik K, Mukherjee A, Mishra MK, De G. Stable Ni nanoparticle-reduced graphene oxide composites for the reduction of highly toxic aqueous Cr(VI) at room temperature. Langmuir. 2014;30(11):3209-16.
62. Shen J, Shi M, Yan B, Ma H, Li N, Ye M. Ionic liquid-assisted one-step hydrothermal synthesis of TiO2-reduced graphene oxide composites. Nano Research. 2011;4(8):795-806.
63. Turcheniuk K, Boukherroub R, Szunerits S. Gold–graphene nanocomposites for sensing and biomedical applications. J Mater Chem B. 2015;3(21):4301-24.
64. Rusi, Majid SR. Green synthesis of in situ electrodeposited rGO/MnO2 nanocomposite for high energy density supercapacitors. Sci Rep. 2015;5:16195.
65. Yu P, Qian Q, Wang X, Cheng H, Ohsaka T, Mao L. Potential-controllable green synthesis and deposition of metal nanoparticles with electrochemical method. Journal of Materials Chemistry. 2010;20(28):5820.
66. Wang B, Li S, Li B, Liu J, Yu M. Facile and large-scale fabrication of hierarchical ZnFe2O4/graphene hybrid films as advanced binder-free anodes for lithium-ion batteries. New J Chem. 2015;39(3):1725-33.

67. Wu X, Wang B, Li S, Liu J, Yu M. Electrophoretic deposition of hierarchical Co3O4@graphene hybrid films as binder-free anodes for high-performance lithium-ion batteries. RSC Adv. 2015;5(42):33438-44.
68. An SJ, Zhu Y, Lee SH, Stoller MD, Emilsson T, Park S, et al. Thin film fabrication and simultaneous anodic reduction of deposited graphene oxide platelets by electrophoretic deposition. The Journal of Physical Chemistry Letters. 2010;1(8):1259-63.
69. Plyasova LM, Molina IY, Gavrilov AN, Cherepanova SV, Cherstiouk OV, Rudina NA, et al. Electrodeposited platinum revisited: Tuning nanostructure via the deposition potential. Electrochimica Acta. 2006;51(21):4477-88.
70. Besra L, Liu M. A review on fundamentals and applications of electrophoretic deposition (EPD). Progress in Materials Science. 2007;52(1):1-61.
71. Thomas BJC, Boccaccini AR, Shaffer MSP. Multi-Walled Carbon Nanotube Coatings Using Electrophoretic Deposition (EPD). Journal of the American Ceramic Society. 2005;88(4):980-2.
72. Girishkumar G, Rettker M, Underhile R, Binz D, Vinodgopal K, McGinn P, et al. Single-wall carbon nanotube-based proton exchange membrane assembly for hydrogen fuel cells. Langmuir. 2005;21(18):8487-94.
73. Burk JJ, Buratto SK. Electrodeposition of Pt Nanoparticle Catalysts from H2Pt(OH)6and Their Application in PEM Fuel Cells. The Journal of Physical Chemistry C. 2013;117(37):18957-66.
74. Novoselov KS, Geim AK, Morozov SV, Jiang D, Zhang Y, Dubonos SV, et al. Electric field effect in atomically thin carbon films. science. 2004;306(5696):666-9.
75. Affoune A, Prasad B, Sato H, Enoki T, Kaburagi Y, Hishiyama Y. Experimental evidence of a single nano-graphene. Chemical Physics Letters. 2001;348(1):17-20.
76. Ishikawa R, Ko PJ, Kurokawa Y, Konagai M, Sandhu A. Electrophoretic deposition of high quality transparent conductive graphene films on insulating glass substrates. Journal of Physics: Conference Series. 2012;352:012003.
77. Hasan SA, Rigueur JL, Harl RR, Krejci AJ, Gonzalo-Juan I, Rogers BR, et al. Transferable graphene oxide films with tunable microstructures. Acs Nano. 2010;4(12):7367-72.

78. Ordikhani F, Ramezani Farani M, Dehghani M, Tamjid E, Simchi A. Physicochemical and biological properties of electrodeposited graphene oxide/chitosan films with drug-eluting capacity. Carbon. 2015;84:91-102.
79. Choi H, Hwang S, Bae H, Kim S, Kim H, Jeon M. Electrophoretic graphene for transparent counter electrodes in dye-sensitised solar cells. Electronics Letters. 2011;47(4):281.
80. Xia X, Tu J, Mai Y, Chen R, Wang X, Gu C, et al. Graphene sheet/porous NiO hybrid film for supercapacitor applications. Chemistry. 2011;17(39):10898-905.
81. Sahoo PK, Aepuru R, Panda HS, Bahadur D. Ice-templated synthesis of multifunctional three dimensional graphene/noble metal nanocomposites and their mechanical, electrical, catalytic, and electromagnetic shielding properties. Sci Rep. 2015;5:17726.
82. Stevens DA, Dahn JR. Electrochemical Characterization of the Active Surface in Carbon-Supported Platinum Electrocatalysts for PEM Fuel Cells. Journal of The Electrochemical Society. 2003;150(6):A770.
83. Ferrari AC, Robertson J. Interpretation of Raman spectra of disordered and amorphous carbon. Physical review B. 2000;61(20):14095.
84. Sobon G, Sotor J, Jagiello J, Kozinski R, Zdrojek M, Holdynski M, et al. Graphene oxide vs. reduced graphene oxide as saturable absorbers for Er-doped passively mode-locked fiber laser. Optics express. 2012;20(17):19463-73.
85. Luo D, Zhang G, Liu J, Sun X. Evaluation Criteria for Reduced Graphene Oxide. The Journal of Physical Chemistry C. 2011;115(23):11327-35.